J Solid State Electrochem (2009) 13:599–608
DOI 10.1007/s10008-008-0760-7

ORIGINAL PAPER

Solid state spectroelectrochemistry of microparticles of ruthenium diimine complexes immobilised on optically transparent electrodes

Gregory J. Barbante · Conor F. Hogan · Andrew B. Hughes

Received: 12 August 2008 / Revised: 25 November 2008 / Accepted: 1 December 2008 / Published online: 17 December 2008

Abstract The solid state electrochemistry and solid state spectroelectrochemistry of two ruthenium complexes, ruthenium tris-(4,7-diphenyl-1,10-phenanthroline) bis-hexafluorophosphate, $[Ru(dpp)_3](PF_6)_2$, and ruthenium bis-(2,2′-bipyridine)(4,6-diphenyl-2,2′-bipyridine)bis-hexafluorophosphate, $[Ru(bpy)_2(dpb)](PF_6)_2$, is described. Microparticles of the material are immobilised on ITO electrodes, and stable voltammetric signals are obtained in contact with aqueous electrolyte solution. Spectral changes monitored during a slow cyclic voltammetric scan confirm the exhaustive oxidation of the Ru^{2+} species to the Ru^{3+} form. The derivative of the absorbance signal monitored at a single wavelength during potential cycling is morphologically identical to a cyclic voltammogram with no background current. This technique is shown to be useful when peaks of small magnitude are obscured by capacitive background or when peaks close to the solvent limit are obscured by solvent electrolysis current. The technique effectively widens the electrochemical window available for voltammetric measurements. After suitable correction of the signal, the value of the voltammetric peak height (I_p) as well as peak potential (E_p) may be obtained from the derivative absorbance signal. Chronospectrometry is demonstrated to provide the equivalent to a chronocoulometric response, but is closer to the ideal simulated response. A facile method for simulating time or potential-dependant spectroelectrochemical responses using commercial electrochemical simulation software is described. Absorbance transients monitored during the electrolysis of solid particles of $[Ru(dpp)_3](PF_6)_2$ show best agreement with simulated data at very short and very long timescales. This observation, in conjunction with the observations from the potential scan experiments, suggests that the absorbance, charge, or current vs. time behaviour of the system can be adequately described by a semi-infinite diffusional model at short experimental timescales and by a finite diffusional model at sufficiently long timescales.

Keywords Voltammetry of microparticles · Ruthenium diimine complexes · UV-Vis spectroelectrochemistry · Optically transparent electrodes · Derivative cyclic voltabsorptometry · Chronospectrometry

Introduction

The use of optically transparent electrodes (OTEs) for in situ spectral monitoring of electrochemical processes represents a powerful combination of techniques. Spectroelectrochemistry has been used not only for the identification of electrogenerated products but has been successfully applied to the delineation of both homogeneous and heterogeneous kinetics and the evaluation of thermodynamic parameters [1–4]. While the majority of such investigations have focused on solution phase systems, spectroelectrochemical approaches have also been used successfully in the characterization of modified electrodes. For example, in the field of bioelectrochemistry, derivative cyclic voltabsorptometry (DCVA), where the derivative of

Electronic supplementary material The online version of this article (doi:10.1007/s10008-008-0760-7) contains supplementary material, which is available to authorized users.

Dedicated to the 80th birthday of Keith B. Oldham.

G. J. Barbante · C. F. Hogan (✉) · A. B. Hughes
Department of Chemistry, La Trobe University,
Melbourne, Victoria 3086, Australia
e-mail: c.hogan@latrobe.edu.au

the optical signal is monitored with respect to an applied triangular potential waveform [5], has been used for the study of redox proteins immobilized on electrode surfaces [6, 7]. DCVA is particularly useful in this area because the signal is morphologically identical to a background-free cyclic voltammogram.

Voltammetry of microparticles, where a solid in microparticulate or microcrystalline form, is immobilized on an electrode surface, in contact with an electrolyte phase in which the material is insoluble, has proved to be a highly effective approach to the investigation of electrochemical processes in solids [8–12]. In situ combinations of spectroscopic techniques such as UV-VIS absorbance [13], X-ray diffraction [14] and diffuse reflectance [15, 16] with this methodology, significantly augment and enhance the efficacy of the approach in the characterization of solid-state processes. In situ UV-VIS absorbance solid-state spectroelectrochemistry is particularly relevant to the characterization of materials for electrochromic applications. Ruthenium diimine complexes possess a unique combination of redox and photophysical properties which make them useful for a wide variety of applications, such as photocatalysis, photoconversion, sensors [17] and light-emitting devices [18]. Despite the fact that most of these applications utilize ruthenium complexes in solid form, the vast majority of investigations into these species has been in solution phase.

In this contribution, we describe the application of DCVA and chronospectrometry (CS) to the solid state electrochemical characterization of ruthenium tris-(4,7-diphenyl-1,10-phenanthroline) bis-hexafluorophosphate, $[Ru(dpp)_3](PF_6)_2$, and a novel complex, ruthenium bis-(2,2′-bipridine)(4,6-diphenyl-2,2′-bipyridine)bis-hexafluorophosphate, $[Ru(bpy)_2(dpb)](PF_6)_2$. Our rationale for examining the spectroelectrochemical properties of these particular compounds is that they are instances of the two most important classes of ruthenium diimine complexes, i.e., those of phenanthroline and bipyridine. $[Ru(bpy)_2(dpb)]^{2+}$ is similar in structure to $[Ru(bpy)_3]^{2+}$, but made hydrophobic by the substitution of phenyl groups on one of the bipyridine ligands. Substitution of one of the phenyl groups at the 6-position rather than placing both at the 4-positions, mitigates the electron-withdrawing effect, thus providing a means of altering the hydropobicity, while substantially retaining the electrochemical and spectroscopic properties of the parent complex. The luminescence of $[Ru(dpp)_3]^{2+}$ is well known, and it has important applications, in immobilised format, in oxygen sensing [19] and solid state light-emitting devices [18]. A full account of the solid state electrochemical, electrochemiluminescent (ECL) and charge transport properties of $[Ru(dpp)_3]^{2+}$ will be presented elsewhere (Barbante et al., manuscript in preparation). Here, we focus on the use of solid state spectroelectrochemical techniques to characterize such materials. Ruthenium$(N)_6$ species generally have high oxidation potentials; the motivation for using DCVA and CS was driven in part by the difficulty, under some circumstances, of obtaining clear solid state voltammetric signals for these materials due to the proximity of their peaks to the solvent limit. We demonstrate also the possibility of obtaining peak height as well as peak potential data from appropriately corrected responses and the equivalent of a "pure" CV in which the signal is solely due to the redox reaction under study.

Experimental

Instrumentation and apparatus The electrochemical measurements were carried out using a CH instruments model 660B or 620C electrochemical workstation. Solution phase electrochemical experiments were performed in a conventional three-electrode cell where the working electrode was a 3-mm diameter glassy carbon (GC) disk electrode (CH Instruments). The data interval was 1 mV or less for all voltammetric experiments and 1 ms or less for all potential step experiments. Spectro-electrochemical measurements were made using a 1-cm cuvette as the electrochemical cell. This consisted of a transparent 5 cm × 0.9 cm indium tin oxide (ITO)-coated glass slide (Aldrich) as the working electrode with the active area (~1.8 cm^2) defined by shrouding part of the conductive surface with Teflon tape. The electrode was held flush against the inner face of the cuvette, with the conductive side facing the solution, such that it was maintained perpendicular to the beam. Numerical smoothing and differentiation were carried out on the absorbance data using a 15- or 17-point Savitsky–Golay algorithm except in the case of the chronospectrometry data which were not smoothed. The data interval was 12.5 ms or less for single wavelength, absorbance–time experiments and 1 nm for UV/VIS spectra.

A Ag/AgCl (3 M KCl) reference electrode was employed for solid state electrochemistry in aqueous media, and a silver wire quasi-reference electrode was used for solution phase experiments in organic media. In this case, the potentials were referenced to the formal potential of the ferrocene/ferrocenium couple measured in situ. A platinum wire or gauze served as the counter electrode in each case. Simulation of transient electrochemical (and absorbance) data was performed using the electrochemical simulation software, DigiElch [20] (version 4, build 2.704).

All solutions were deoxygenated using grade 5 nitrogen between 10 and 15 min prior to electrochemical experiments. The GC working electrodes were polished prior to each experiment using BUEHLER Microcloth® Polishing Cloth with aqueous slurries of 0.3 and 0.05 μm alumina.

ITO electrodes were sonicated for 5 min in Milli Q water and then left to dry prior to electrochemical experiments. All measurements were carried out at ambient temperature (20± 2 °C). UV/Vis spectra were recorded using an Ocean Optics USB2000 USB-ISS-UV/Vis spectrometer with OOIBase32 software or on a Varian Cary UV/Vis spectrometer with Eclipse software. Fluorescence spectra were recorded on Varian Cary Eclipse fluorescence spectrometer. Mass spectra were recorded using Electrospray ionisation with an ion trap on a Brüker Esquire 6000 mass spectrometer. Electrospray mass spectrometry (ESMS) was performed on a Fission VG Bio-Q electrospray mass spectrometer. Infrared spectra (IR) were recorded on a Shimadzu Fourier transform-infrared spectroscopy. Nuclear magnetic resonance (NMR) spectra were performed in *d*-chloroform, *d*-acetonitrile or D_6-DMSO on a Brüker AM-300 Spectrometer. All melting points were uncorrected and performed on a Reichert "Thermopan" microscope hot-stage apparatus. Thin-layer chromatography was performed on Merk kieselgel 60 F254 plates and visualised with a 254-nm UV lamp.

Electrode modification For solid state voltammetric measurements, the complexes were immobilised on the working electrode by drop coating 1 to 2 μL of a cold (4 °C) 1.0 mM solution of the ruthenium complex dissolved in acetone. On ITO electrodes, the area covered by deposition solution (0.2 to 0.5 cm^2) was defined by drop coating over a Teflon tape mask. The layer was left to dry on the electrode surface in an enclosed container for 4 to 6 h before removing the mask and performing electrochemical experiments. Atomic force microscopy measurements showed that this method of immobilization resulted in an array of submicron-sized particles on the electrode surface (Barbante et al., manuscript in preparation).

Materials All reagents were of analytical grade or higher and were purchased from Sigma-Aldrich. Electrochemical grade $[Bu_4N][PF_6]$ and $LiClO_4$ electrolytes were used, and organic solvents were distilled and stored over 4 Å molecular sieves prior to use. Aqueous solutions were prepared using deionised water (18 MΩ cm^{-1}).

Synthesis Ruthenium tris-(4,7-diphenyl-1,10-phenanthroline) bis-hexafluorophosphate, $[Ru(dpp)_3](PF_6)_2$) was synthesized according to a modified literature procedure [21]. ^{1}H NMR (300 MHz, $CDCl_3$) δ 7.52–7.59 (m, 10H aromatic), 7.79 (d, 3H aromatic), 8.21 (s, 3H aromatic), 8.37 (d, 3H aromatic) (see supplementary Figure 5). ESMS: *m/z* $[M-2PF6]^+$ 549.5 (Calcd. for $C_{78}H_{48}Ru$: 549.2).

The substituted bipyridine ligand, 4,6-diphenyl-2,2'-bipyridine (dpb) was also prepared using literature procedures [22–25].

Ruthenium bis-(2,2′-bipyridine)(4,6-diphenyl-2,2′-bipyridine)bis-hexafluorophosphate, $[Ru(bpy)_2(dpb)](PF_6)_2$. Ruthenium bis-(2,2′-bipyridine) dichloride (0.16 g, 0.32 mmol) and 4,6-diphenyl-2,2′-bypridine (0.10 g, 0.33 mmol) were dissolved in a mixture of ethanol and water (20 ml, 3:1), respectively, and refluxed for 2 h in a nitrogen atmosphere. Once a deep red solution had formed, the solution was evaporated at reduced pressure, and then the crude product was redissolved in MilliQ water (10 ml). The resulting red solution was then suction filtered through a Buchner funnel, and the filtrate was treated with saturated aqueous KPF_6 to precipitate the ruthenium polypyridyl complex. The resulting orange precipitate was then suction filtered and was washed with water (2×10 ml) and ether (2×10 ml). Recrystallisation from acetone:water mixture (2:1); the orange powder was then suction filtered using a sintered funnel and was then washed with ether (10 ml) and dried under vacuum to yield (0.13 g, 79%). IR (KBr) ν_{max} (aromatic C=C) 3087, 1612, 1482, 1466, 1446, 1424, 1414, 1400; ^{1}H NMR (300 MHz, DMSO-d_6) δ 6.01 (brd s, 1H, aromatic), 6.65 (brd s, 1H, aromatic), 6.86–6.94 (m, 4H, aromatic), 7.33 (d, *J* 4.16, 3H, aromatic), 7.44 (t, *J* 6.35, 1H, aromatic), 7.51–7.67 (m, 7H, aromatic), 7.73 (s, 1H, aromatic), 7.81 (d, *J* 5.3, 1H, aromatic), 8.01 (q, *J* 4.7,1H, aromatic), 8.15–8.28 (m, 7H, aromatic), 8.61–8.72 (m, 3H, aromatic), 9.18–9.23 (m, 2H, aromatic). ^{13}C NMR (75 MHz, DMSO-d_6) δ 120.49, 123.3, 124.35, 124.50, 126.01, 126.51, 127.32, 127.50, 127.80, 128.10, 128.95, 129.40, 130.92, 134.56, 135.98, 137.86, 138.04, 138.11, 138.71, 148.31, 150.56, 151.14, 151.34, 152.8, 155.93, 156.69, 156.74, 157.59, 157.78, 157.85, 166.31; ESI-MS: *m/z* $[M\text{-}PF_6^-]^+$ 867.2 (Calcd for $C_{42}H_{32}N_6RuPF_6$: 866.7). See supplementary Figures 2, 3 and 4 for mass spectrometry (MS) and NMR spectra.

Results and discussion

Solution phase properties

The voltammetric and spectroscopic data for $[Ru(bpy)_2(dpb)_3]^{2+}$, $[Ru(dpp)_3]^{2+}$ and $[Ru(bpy)_3]^{2+}$ dissolved in acetonitrile containing 0.1 M $[Bu_4N][PF_6]$ as supporting electrolyte are summarized in Table 1. The voltammogram for $[Ru(bpy)_2(dpb)]^{2+}$ (see supplementary material, Figure 1) is typical for ruthenium $(N)_6$ complexes. The peaks centred at 0.85 V (vs. Fc) (process I) are due to the oxidation/reduction of the metal between the 2+ and the 3+ state, while the three processes (II, III, and IV), at more negative potentials, are attributed to the successive reductions of the ligands. The third reduction process (IV), is assigned to the

Table 1 Solution phase and solid state electrochemical and spectroscopic properties

	Solution phase						Solid state[c]		
	$E°/V$(vs. Fc)[a]				λ_{em}[b]/nm	λ_{abs}/nm	$E_{1/2}$[d]/V	λ_{em}[b]/nm	λ_{abs}/nm
	I	II	III	IV					
$[Ru(dpp)_3]^{2+}$	0.85	−1.70	–	–	616	464	1.14	637	464
$[Ru(dpb)(bpy)_2]^{2+}$	0.88	−1.68	−1.90	−2.21	618	454	1.15	–	462
$[Ru(bpy)_3]^{2+}$	0.89	−1.75	−1.94	−2.18	620	452	1.1[e]	–	–

[a] $E°$ (ferrocene) was approximately 0.32 V vs. Ag/AgCl
[b] Emission spectra in CH_3CN. Responses corrected for variation in detector sensitivity with wavelength
[c] Immobilized on ITO electrode, in contact with 0.1 M $LiClO_4$
[d] vs. Ag/AgCl(3MKCl)
[e] From reference [16], in 0.1 M NaF

phenyl-substituted ligand, consistent with the electron-donating ability of this substituent. The spectroscopic properties for $[Ru(bpy)_2(dpb)]^{2+}$ presented in Table 1 are also characteristic of ruthenium(tris)diimine complexes. Like $[Ru(bpy)_3]^{2+}$ and $[Ru(dpp)_3]^{2+}$, the absorption band in the visible region is due to a metal to ligand charge transfer (MLCT), while the photoluminescent emission originates from a triplet state, populated by efficient intersystem crossing from the singlet. Two further absorption bands are observed in the UV region at 290 and 246 nm which are assigned to ligand-centred (π-π^*) transitions.

Solid state electrochemistry Fig. 1 illustrates the cyclic voltammetric responses at various scan rates, for layers of microparticles of $[Ru(dpp)_3](PF_6)_2$ (upper graph) and $[Ru(bpy)_2(dpb)](PF_6)_2$ (lower graph), immobilized on ITO electrodes where the supporting electrolyte is 0.1 M $LiClO_4$. The response for $[Ru(dpp)_3](PF_6)_2$ is similar to that observed on glassy carbon substrate which will be described elsewhere (Barbante et al., manuscript in preparation). The solid state redox process in both cases is assumed to involve the transfer of both electrons and ions as follows:

$$\left[\mathbf{Ru(L)_3}\right]^{2+}[\mathbf{A}^-]_{2(\text{solid})}+[\mathbf{A}^-]_{(\text{solution})} \leftrightarrow \left[\mathbf{Ru(L)_3}\right]^{3+}[\mathbf{A}^-]_{3(\text{solid})}+\mathbf{e}^- \quad (1)$$

Where L is a diimine ligand and A^- is the ClO_4^- or PF_6^- counterion which enters or leaves the solid to maintain electroneutrality on redox switching.

The solid state voltammetry of both complexes exhibited a pronounced "break-in" effect, where the peak current gradually increased in magnitude during continuous cycling, before reaching a steady state, typically after 20–50 cycles. The voltammograms in Fig. 1 represent the response after the solid deposits had been repeatedly cycled until an unchanging response was obtained. After the break-in period, the layers showed excellent stability typically with <10% decrease in peak currents after 100 voltammetric cycles at 0.1 V s^{-1}. The insets in Fig. 1 show that at moderately fast scan rates (0.1–0.5 V s^{-1}), the magnitude of the peak currents for both complexes scales linearly with the square root of scan rate. At these scan rates also, the peaks exhibit tailing, reminiscent of a diffusional response, such as that obtained for the freely diffusing complex. Although, due to ohmic effects, the peak to peak splitting (ΔE_p) is somewhat larger in the CV for the immobilised material. At slower scan rates (0.005–0.05 V s^{-1}), the peak heights scale linearly with scan rate and are more symmetrical in shape. These observations suggest that charge percolation through these deposits can be treated as a diffusion-like process where the electrochemical reaction is assumed to start at the three-phase electrode–particle–solution boundary, and the subsequent growth of the reaction zone follows a semi-infinite linear diffusion into the particles [16]. Moreover, finite diffusional (thin layer) type behaviour may be exhibited at sufficiently long experimental timescale.

Solid state spectroelectrochemistry Fig. 2 shows the changes in the visible absorption spectrum of a low surface coverage ($\Gamma=1.5\times10^{-9}$ mol cm^{-2}) layer of immobilized particles of $[Ru(dpp)_3](PF_6)_2$, during a slow (10 mV s^{-1}) linear scan voltammetric experiment between 0.5 and 1.5 V vs. Ag/AgCl. Oxidation of Ru^{2+} to Ru^{3+} within the solid deposit is signalled by a gradual decrease in the intensity of the MLCT band at 464 nm and the growth of a shoulder at 380 nm, which is due to a metal-centred (MC) transition [26]. The clear isosbestic point observed at 400 nm indicates that no other products are generated during the electrolysis. Experiments where the potential was maintained at 1.5 V, at the conclusion of the scan, for up to 60 s resulted in no further changes to the spectrum. When a 1-mM solution of the complex dissolved in acetonitrile was oxidized in a thin-layer cell using a Pt gauze working electrode, a very similar pattern to that observed in the solid

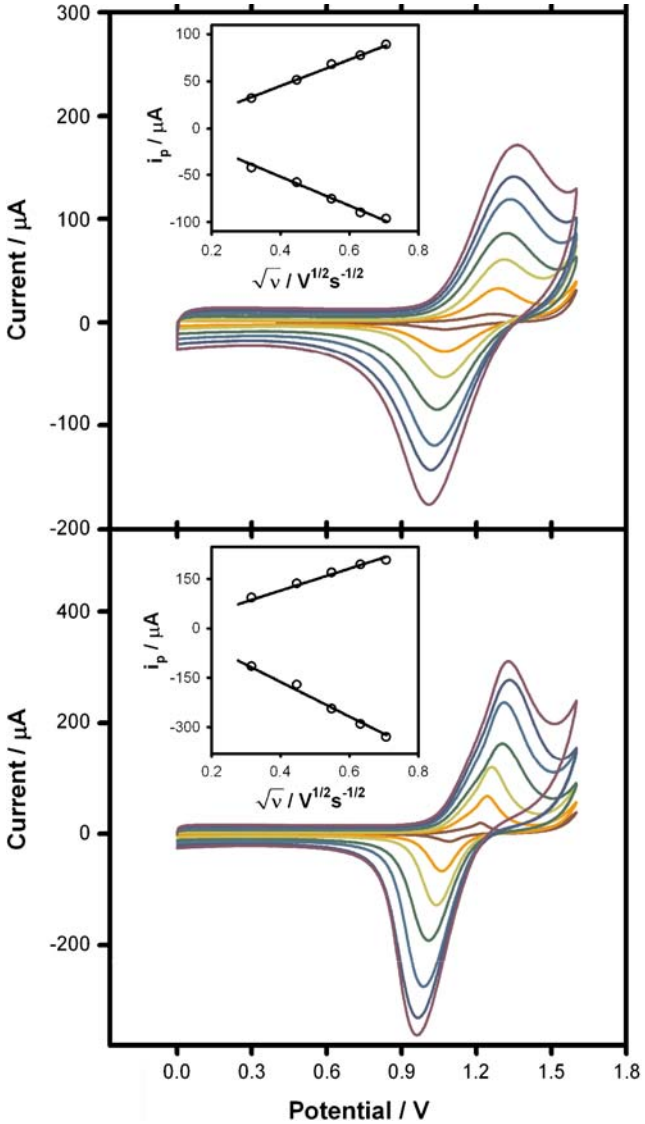

Fig. 1 Scan rate dependences of the solid state cyclic voltammetric responses for deposits of microparticles of $[Ru(dpp)_3](PF_6)_2$ (*upper graph*) and $[Ru(bpy)_2(dpb)](PF_6)_2$ (*lower graph*) immobilized on ITO. The scan rates are 0.01, 0.05, 0.1, 0.2, 0.3, 0.4, and 0.5 V s^{-1} for both plots, the electrode area was 0.25 cm^2 for the *upper graph* and 0.27 cm^2 for the *lower graph* and the supporting electrolyte was 0.1 M $LiClO_4$ in both cases. The *inset* shows the dependence of peak current (I_p) on square root of scan rate between 0.1 and 0.5 V s^{-1} in each case

state experiment is seen. The inset in Fig. 2 which shows the absorbance monitored at 460 nm with respect to time during repetitive potential pulsing, demonstrates that the spectral changes due to oxidation of the solid material are reversible over many cycles. That the MLCT band is lost completely at the end of the scan indicates that the layer is exhaustively oxidized on the timescale of the experiment and further supports the interpretation of the electrochemical behaviour of these deposits in the context of a finite diffusional/thin layer model. Analogous behaviour to that described above was observed for solid deposits of $[Ru(bpy)_2(dpb)](PF_6)_2$ immobilised on ITO.

Another aspect of the spectroelectrochemical approach is where the absorbance signal $A(t,\lambda)$ is monitored at a single wavelength as a function of time or applied potential. Since both $A(t,\lambda)$ and the faradaic charge $Q(t)$ represent the integral of the flux of Eq. 1 [27], the derivative of the absorbance with respect to time is directly related to that of the charge with respect to time, namely, the current $I(t)$, [5] i.e.,

$$\frac{dA(t,\lambda)}{dt} = I(t)\frac{\varepsilon}{nFa} \tag{2}$$

where a is the electrode area in cm^2, the other symbols have their usual meaning. Thus $dA(\lambda,t)/dt$ provides an alternative measure of the flux associated with the redox reaction and, in contrast to the electrochemical signal, does so with both insensitivity to non-faradaic charge-consuming processes and enhanced molecular specificity associated with the use of spectroscopic techniques.

Because, in the system under study here, both the oxidised and reduced forms of the materials absorb at the wavelength of analysis, the true absorbance due to the Ru^{2+} form alone must be extracted from the data if quantitative information is required. This can be readily accomplished, if the absorptivities of both species are known, by applying

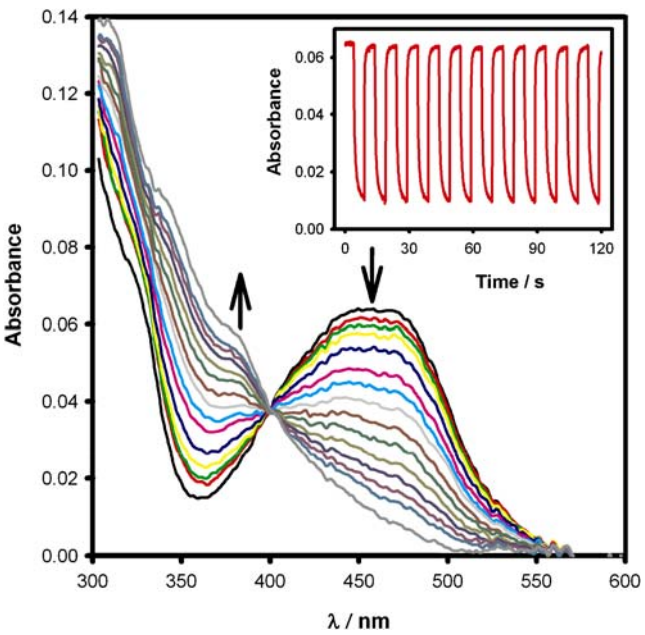

Fig. 2 Changes in solid state UV-Vis absorbance spectrum of a layer of $[Ru(dpp)_3](PF_6)_2$ microparticles immobilised on ITO in contact with 0.1 M $LiClO_4$, during slow voltammetric scan between 0.5 and 1.5 V vs. Ag/AgCl. The *inset* shows the absorbance signal monitored at 460 nm during repetitive pulsing of the applied potential between 0.5 and 1.5 V

an appropriate correction factor. This is derived below for the present situation, where the decrease in absorbance due to electrolysis of a species is being monitored. A similar argument applies for systems where the absorbance of an electrolysis product is monitored. Firstly, the total absorbance at any given wavelength and time is given by

$$A = \varepsilon_{Ru^{2+}}\Gamma_{Ru^{2+}} + \varepsilon_{Ru^{3+}}\Gamma_{Ru^{3+}} \quad (3)$$

where $\Gamma_{Ru^{2+}}$ and $\Gamma_{Ru^{3+}}$ are the surface concentrations (mol cm^{-2}) of the oxidised and reduced forms of the complex. Since, at any time, the total surface coverage Γ_T is given by

$$\Gamma_T = \Gamma_{Ru^{2+}} + \Gamma_{Ru^{3+}} \quad (4)$$

Substituting for $\Gamma_{Ru^{2+}}$, we get

$$A = \varepsilon_{Ru^{3+}}\Gamma_{Ru^{3+}} + \varepsilon_{Ru^{2+}}(\Gamma_T - \Gamma_{Ru^{3+}})$$
$$= \varepsilon_{Ru^{3+}}\Gamma_{Ru^{3+}} + \underline{\underline{\varepsilon_{Ru^{2+}}\Gamma_T}} - \varepsilon_{Ru^{2+}}\Gamma_{Ru^{3+}} \quad (5)$$

Prior to electrolysis, the initial absorbance is described by, $A_i = \varepsilon_{Ru^{2+}}\Gamma_T$, so the change in the absorbance signal, ΔA is given by

$$\Delta A = A - A_i = \varepsilon_{Ru^{3+}}\Gamma_{Ru^{3+}} - \varepsilon_{Ru^{2+}}\Gamma_{Ru^{3+}}$$
$$= (\varepsilon_{Ru^{3+}} - \varepsilon_{Ru^{2+}})\Gamma_{Ru^{3+}} \quad (6)$$

or

$$\Gamma_{Ru^{3+}} = \frac{\Delta A}{\varepsilon_{Ru^{3+}} - \varepsilon_{Ru^{2+}}} \quad (7)$$

Therefore, the absorbance due to Ru^{3+} is given by

$$A_{Ru^{3+}} = \Delta A\left(\frac{\varepsilon_{Ru^{3+}}}{\varepsilon_{Ru^{3+}} - \varepsilon_{Ru^{2+}}}\right) \quad (8)$$

Since the absorbance due to Ru^{2+} alone is described by, $A_{Ru^{2+}} = A - A_{Ru^{3+}}$, it follows that

$$A_{Ru^{2+}} = \Delta A\left(\frac{\varepsilon_{Ru^{2+}}}{\varepsilon_{Ru^{2+}} - \varepsilon_{Ru^{3+}}}\right) + A_i \quad (9)$$

The absorptivities $\varepsilon_{Ru^{2+}}$ and $\varepsilon_{Ru^{3+}}$ were determined by measuring the absorbance before and after exhaustive oxidation of the attached solid in a slow scan rate voltammetric experiment, such as that shown in Fig. 3. Q_T (and thus Γ_T) was evaluated from the area under the background corrected voltammetric peak. The values obtained for $\varepsilon_{Ru^{2+}}$ and $\varepsilon_{Ru^{3+}}$ for $[Ru(dpp)_3]^{2+}$ were 3.15 ($\pm$0.20)$\times 10^7$ cm^2 mol^{-1} and 5.66($\pm$0.25)$\times 10^6$, respectively, giving a correction factor of 1.219. The absorptivity of the reduced form of the solid is similar to the value of 2.95×10^7 cm^2 mol^{-1} (or 29,500 M^{-1} cm^{-1}) obtained for the complex dissolved in acetonitrile.

The upper graph in Fig. 3 shows the voltammetric response (dotted line) at a slow scan rate for a layer of immobilised microparticles of $[Ru(dpp)_3](PF_6)_2$. The simultaneously collected absorbance signal at 460 nm (solid line) is also shown with the correction factor $\frac{\varepsilon_{Ru^{2+}}}{\varepsilon_{Ru^{2+}}-\varepsilon_{Ru^{3+}}}$, from Eq. 9 above, applied. The lower graph of Fig. 3 represents the derivative (dA/dE) of the corrected absorbance signal shown in the upper curve. Plots of this type are often referred to as derivative cyclic voltabsorbtammograms, (DCVA) [5]. The data has been multiplied by the factor $\frac{nFav}{\varepsilon}$ from Eq. 2, to show the equivalence of, and allow direct comparison of, the voltammetric and spectroscopic signals. (The scan rate, ν, simply converts between dA/dE and dA/dt). Unlike the current, which includes contributions from capacitive charging and other background processes, the derivative absorbance signal originates solely from the redox processes embodied in Eq. 1. If the derivative in Fig. 3, is regarded then, as a perfectly background subtracted voltammogram, both signals are in satisfactory agreement with one another. Drawing a linear baseline between both sides of the foot of the voltammetric peak gives a value of 7.5 μA for the peak current (I_p), whereas the peak derivative signal $(dA/dV)_p$, when multiplied by the factor nFAν/ε, has a value of 6.7 μA.

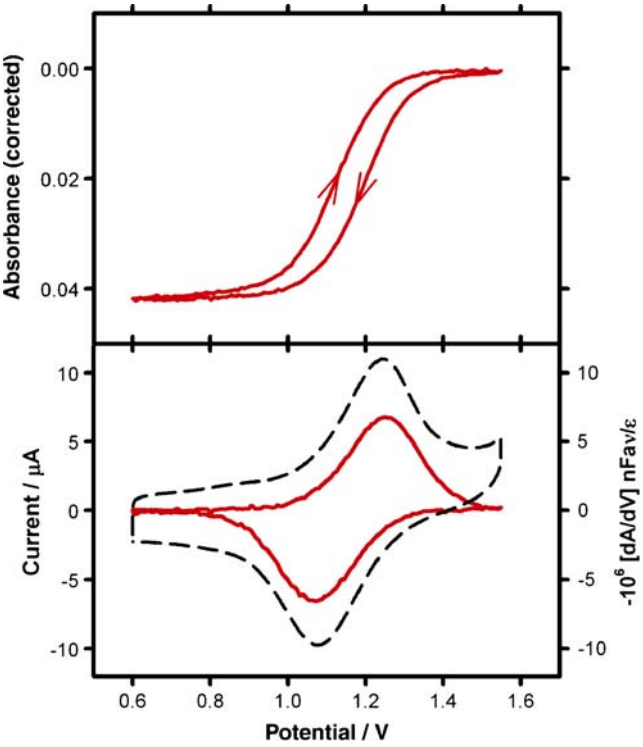

Fig. 3 Cyclic voltabsorptometry (*upper graph*), derivative cyclic voltabsorptometry (DCVA) (*lower graph*) and cyclic voltammetry (*lower graph*) for immobilised microparticles of $[Ru(dpp)_3](PF_6)_2$. Scan starts at 0.6 V, the scan rate (ν) is 0.05 V s^{-1}, the electrode area (a) is 0.25 cm^2, the surface coverage (Γ_T) is 1.32×10^{-9} mol cm^{-2}, and the absorptivity of the Ru^{2+} form of the solid (ε) is 3.15×10^7 cm^2 mol^{-1}. The absorbance signal was corrected to account for the absorbance of the Ru^{3+} species according to Eq. 9

Figure 4 shows the CV and DCVA responses for a layer of immobilised $[Ru(dpp)_3](PF_6)_2$ at the relatively fast scan rate of 0.5 V s^{-1}. Also, the surface coverage, and therefore the thickness of the deposit, in this experiment is somewhat higher than the case in Fig. 3. A feature of these materials which we have noted is that the voltammetric peaks become less distinct and smaller in magnitude relative to the case for thinner deposits cast from a smaller volume of deposition solution. This is presumably related to an impediment to the flux of charge compensating counterions in the thicker deposits, resulting in a diminished rate of charge transport. As a result of this phenomenon, the forward voltammetric peak in Fig. 4 is poorly resolved from the background making peak height (i_p) or peak potential (E_p) determination a somewhat subjective affair. However, the derivative signal allows both of these parameters to be measured with relative ease. The DCVA signal displays several features which distinguish it from the corresponding signal in Fig. 3. Namely, the peaks exhibit tailing rather than being symmetrical, and the derivative absorbance signal does not return to zero as it does in the slow scan rate experiment. These observations are consistent with a transition to semi-infinite diffusional type behaviour, which one would expect to observe as the timescale of the experiment decreases and/or the thickness of the deposit increases.

This advantage of the spectroelectrochemical approach is further illustrated in Fig. 5. In this case, the potential of the working electrode has been deliberately driven past the solvent limit to 2.0 V vs. Ag/AgCl, where the voltammetric signal consists almost entirely of current due to the electrolysis of the solvent. Care was taken not to scan far enough such as to cause evolution of gas bubbles. As expected under these conditions, the oxidative wave of the

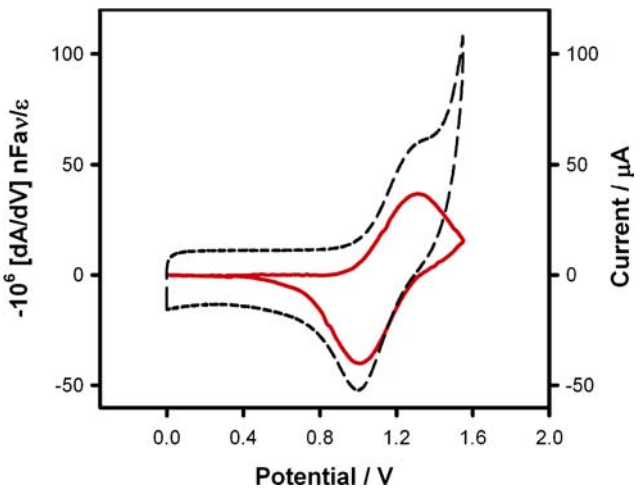

Fig. 4 Solid state CV and DCVA responses for $[Ru(dpp)_3](PF_6)_2$ immobilised on ITO at the scan rate of 0.5 V s^{-1} where the electrode area (a) was 0.2 cm^2 and the surface coverage Γ_T was 5×10^{-9} mol cm^{-2}

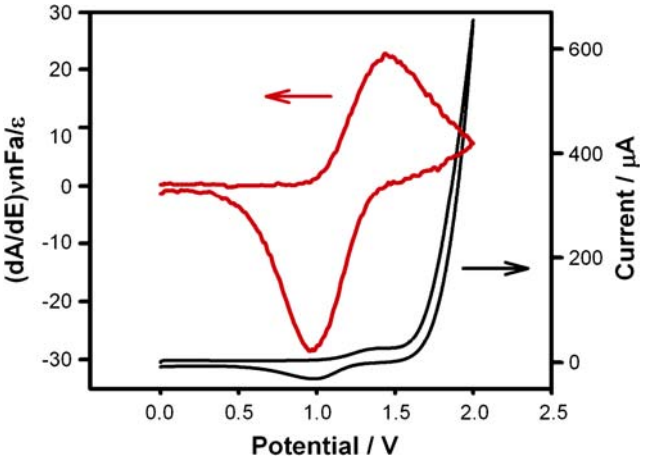

Fig. 5 Solid state CV and DCVA responses for $[Ru(dpp)_3](PF_6)_2$ immobilised on ITO in contact with aqueous 0.1 M $LiClO_4$ at the scan rate of 0.1 V s^{-1} where the potential was reversed at 2.0 V vs. Ag/AgCl. The electrode area was 0.3 cm^2

CV is indistinct with the peak tail significantly convoluted with the solvent electrolysis current. The derivative absorbance signal is however unaffected by this background process and provides a signal morphologically identical to a CV regardless of solvent limit. While acknowledging that the materials under study here can, under most conditions, be studied by conventional techniques without being gravely affected by the solvent limit, the potential applications of this technique in situations where the voltammetric signal is closer to or even buried within the solvent electrolysis current is obvious.

The solid state voltammetric responses and corresponding derivative absorbance responses for a layer of immobilized $[Ru(bpy)_2(dpb)](PF_6)_2$ microparticles at scan rates of 0.005, 0.1, and 0.5 V s^{-1} are shown in Fig. 6. Note that while the peak currents (I_p) in the voltammograms increase with increasing scan rate, the opposite trend applies for the variation of $(dA/dV)_p$ with scan rate, as expected [5]. As observed for $[Ru(dpp)_3](PF_6)_2$, there is a distinct variation in peak shape on going from high to low scan rate. This is most readily seen in the derivative absorbance signals where the slow scan rate gives a narrow and reasonably symmetrical response, whilst the two faster scan rates result in broader tailed peaks. Whilst ohmic effects undoubtedly account for some of the peak broadening, there is little doubt but that the relatively rapid return of the signal to baseline in the slow scan rate response is due to the exhaustive electrolysis of the deposit, consistent with thin layer type behaviour.

Potential step techniques such as chronoamperometry and chronocoulometry are also commonly used in the characterization of modified electrodes. For example, the charge transport characteristics can readily be extracted from a plot of current vs. $t^{-1/2}$ in the case of chronoamperometry or charge vs. $t^{1/2}$ in the case of chronocoulometry.

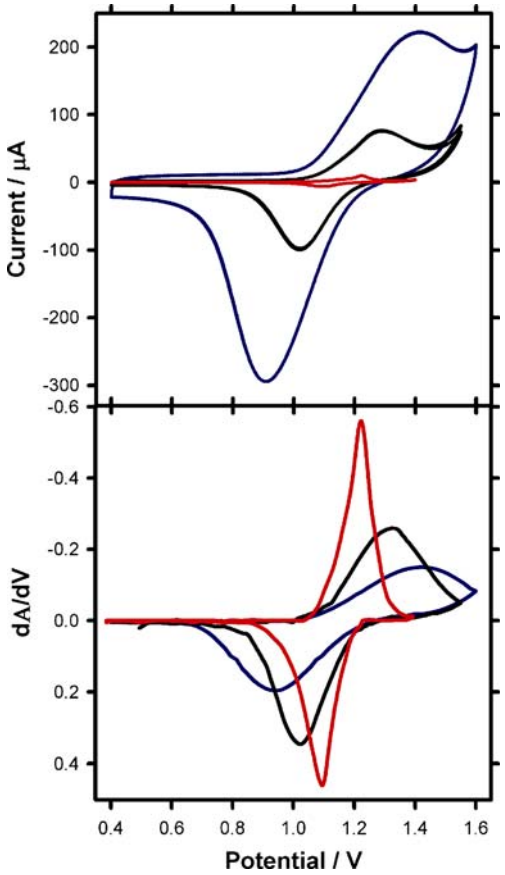

Fig. 6 Solid state voltammetric responses (*upper graph*) and corresponding derivative absorbance responses for a layer of immobilized $[Ru(bpy)_2(dpb)](PF_6)_2$ microparticles at scan rates of 0.005, 0.1 and 0.5 V s^{-1}

Like voltammetry, the efficacy of these techniques may be adversely affected by charge consuming background processes, particularly if, in order to completely step over the wave, it is necessary to step the potential to a value where solvent is electrolysed, as is the case for the ruthenium complexes examined here. Therefore, it is of interest to explore the use of spectroelectrochemical approaches to circumvent such potential problems.

Since the absorbance signal A during electrolysis is directly related to the faradaic charge passed Q, like the analogous relationship used in the coulometric technique, the absorbance transient varies with the square root of time according to [27]

$$A = \frac{2\varepsilon C\sqrt{D_{CT}}\sqrt{t}}{\sqrt{\pi}} \tag{10}$$

where C is the concentration of redox active centres in the deposit, and D_{CT} is the charge transport diffusion coefficient. Therefore, chronocoulometry and its sister technique chronospectrometry may be compared directly without the necessity to derivatise or smooth the data. One advantage of potential step techniques is that, unlike most voltammetric methods, the effect of experimental timescale may be probed in a single experiment. We have compared the responses from these two techniques with simulated spectroelectrochemical data, in order to gauge the relative merits of the two approaches. Chronospectrometry simulations were performed using DigiElch, a commercial software package which uses a box method to perform electrochemical simulations [22]. Since, as mentioned, Q and A both represent the integral of the flux of Eq. 1, the chronospectrometry and chronocoulometry responses ought to be morphologically identical and directly proportional. Therefore, spectroelectrochemical simulations may be performed by inserting the constant $\frac{\varepsilon}{nFa}$ in the space where a, the value of the electrode area, is normally entered, (remembering that the appropriate units of ε are cm^2 mol^{-1}) and digitally integrating the resulting data.

Figure 7 shows the change in absorbance monitored at 460 nm and the accumulation of charge, associated with the oxidation of solid deposits of $[Ru(dpp)_3](PF_6)_2$, with

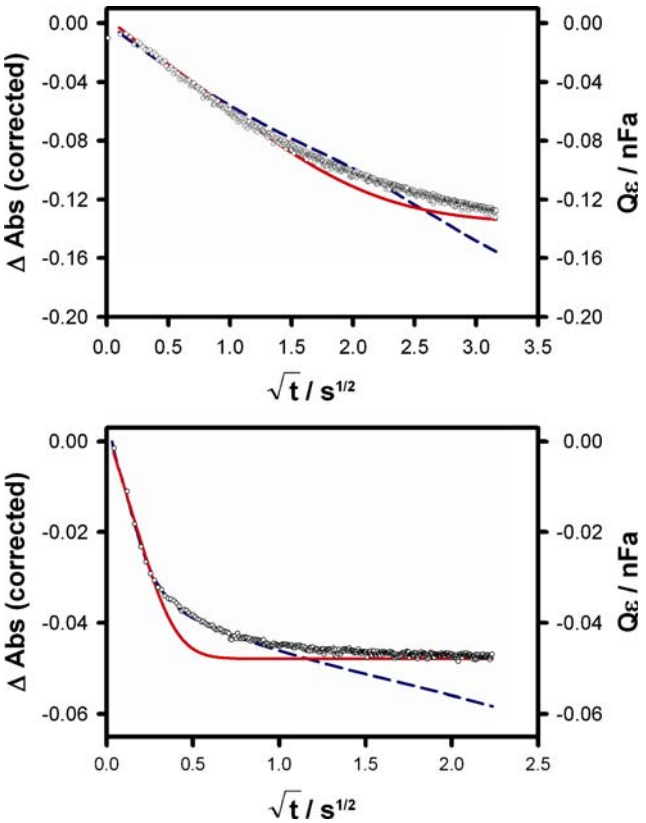

Fig. 7 Chronocoulometry (*dashed line*), chronospectrometry (*open circles*) and simulated chronospectrometry (*solid line*) for high (*upper graph*) and low (*lower graph*) surface coverage $[Ru(dpp)_3](PF_6)_2$ immobilised on ITO in contact with aqueous 0.1 M $LiClO_4$. In the *upper graph*, the electrode area (a) was 0.49 cm^2, and Γ_T was 4.7×10^{-9} mol cm^{-2}. In the lower graph, (a) was 0.45 cm^2, and Γ_T was 1.6×10^{-9} mol cm^{-2}. The absorbance was monitored at 460 nm. Simulation parameters are as stated in the main text

respect to time, during a potential step experiment. The upper and lower graphs represent the response for thick and thin deposits, respectively. The thickness was varied in order to assess the extent to which the layer solution boundary influences the response. In the upper graph where the deposit is thick, both the absorbance and the charge vary linearly with the square root of time up to approximately 1.0 $s^{1/2}$. The chronocoulometry and chronospectrometry slopes from this portion of the graph give values of 1.7×10^{-9} and 1.8×10^{-9} for $\sqrt{D_{CT}}C$, respectively, $\sqrt{D_{CT}}C$ being a measure of the rate of charge transport. These values are in good agreement with chronoamperometric analysis (using the Cottrell equation) which gave a value of 1.8×10^{-9} and CV data from Fig. 1 which gave a value of 2.2×10^{-9} using the Randles Sevcik equation.

At longer times, as the thickness of the depletion layer approaches that of the deposit itself, the absorbance drops below that predicted by Eq. 10, and the charge falls below that predicted by the integrated Cottrell equation. At even longer experimental timescales (greater than 2.0 $s^{1/2}$) whilst the absorbance signal begins to plateau, significantly, the slope of the coulometric signal increases. Since unlike the electrochemical signal, the spectroscopic signal is sensitive only to changes in the concentrations of the ruthenium centres, the apparent excess charge passed at long timescales is most likely associated with background processes such as solvent electrolysis. The solid red line in the upper graph is the simulated spectroscopic response for a layer thickness of 4.3×10^{-6} cm [28]. Both signals are in good agreement with the simulated response at short times. However, at intermediate experimental timescales, the charge deviates significantly both above and below the idealized response, whereas the absorbance exhibits only negative deviations, which get smaller at even longer times.

The lower curve in Fig. 7, where a smaller quantity of material was drop coated on the electrode, and thus, the thickness of the deposit is smaller, also shows good agreement between the optical and electrochemical signal at short times (<0.25 $s^{1/2}$). The slopes of both the electrochemical and spectroscopic signals from this short time portion of the graph yields a value of 3.8×10^{-9} for $\sqrt{D_{CT}}C$, in agreement with our earlier observation of faster charge transport rates for thinner layers. As in the upper graph of Fig. 7, there is significant disagreement between the spectroscopic and electrochemical signals at timescales longer than about 1.0 $s^{1/2}$. While the absorbance reaches a constant value as the deposit becomes fully oxidized, the charge continues to increase, presumably due to charge-consuming processes unrelated to the redox switching of the layer. The simulated response, in good agreement with both signals at short times, is in good agreement with the absorbance signal at both short *and* long times, with some significant deviation at intermediate times. The negative deviation of the absorbance from the model at these intermediate times may be explained by the fact that the model response assumes a perfect layer of uniform thickness with a well-defined layer solution boundary. In reality, however, these deposits are not monolithic and likely contain a distribution of particle sizes, with the result that, the depletion zone may be influenced by the layer solution boundary at intermediate times as well as at longer times, as the more remote portions of the immobilized material are electrolysed over a longer period of time.

Conclusions

The solution phase electrochemical and spectroscopic properties of a novel bipyridine complex of ruthenium, $[Ru(bpy)_2(dpb)]^{2+}$, are similar to those of $[Ru(dpp)_3]^{2+}$ and $[Ru(bpy)_3]^{2+}$. When immobilized on ITO electrodes in the form of microparticles, stable solid state voltammetry is observed for $[Ru(dpp)_3]^{2+}$ and $[Ru(bpy)_2(dpb)]^{2+}$ in contact with aqueous perchlorate electrolyte solution. The peak shapes and scan rate dependence of the peak currents in both systems indicate that charge transport in the particles is semi-infinite diffusional in nature at faster scan rates, while at slow scan rates, a finite diffusional model adequately describes the responses. Spectral changes monitored during a slow cyclic voltammetric scan confirm the exhaustive oxidation of the Ru^{2+} species to the Ru^{3+} form which is signalled by the disappearance of the MLCT band and simultaneous growth of a MC band at lower wavelengths. The spectral changes are reversible over many oxidation–reduction cycles.

The derivative of the absorbance signal monitored at a single wavelength during potential cycling is morphologically identical to a background-free cyclic voltammogram. This technique is shown to be useful when peaks of small magnitude are obscured by capacitive background or when peaks close to the solvent limit are obscured by solvent electrolysis current. The technique effectively increases the electrochemical window available for voltammetric measurements. This will be useful for studies of compounds with high (or low) formal potentials, in cases where oxygen cannot be removed from solution and studies at high or low pH.

Since the relationship between dA/dt and the faradaic current (I) is known, quantitative as well as qualitative information may be obtained under favourable conditions. As both the oxidized (Ru^{3+}) and reduced (Ru^{2+}) species absorb at the wavelength of analysis, a correction factor of $\frac{\varepsilon_{Ru^{2+}}}{\varepsilon_{Ru^{2+}}-\varepsilon_{Ru^{3+}}}$ must be applied. The derivation of this correction factor is also presented.

Chronospectrometry experiments can provide the equivalent to a chronocoulometric response. Moreover, due to the "invisibility" of charge-consuming processes unrelated

to the redox reaction, the response is closer to the ideal simulated response than the electrochemical signal. Spectroelectrochemical responses may be easily simulated using commercially available electrochemical simulation software. Absorbance transients from thick and thin deposits of $[Ru(dpp)_3](PF_6)_2$ on ITO show best agreement with simulated data at very short and very long timescales. This observation, in conjunction with the observations from the potential scan experiments, suggests that the absorbance, charge or current vs. time behaviour of the system can be adequately described by a semi-infinite diffusional model when $\sqrt{2D_{CT}t} \ll$ the average particle size and by a finite diffusional model when $\sqrt{2D_{CT}t} \geq$ the average particle size.

References

1. Kuwana T, Heineman WR (1976) Acc Chem Res 9:241 doi:10.1021/ar50103a001
2. Bancroft EE (1982) J Electrochem Soc 129:298C doi:10.1149/1.2124312
3. Porter MD, Dong S, Gui Y, Kuwana T (1984) Anal Chem 56:2263. doi:10.1021/ac00276a068
4. Zhang C, Park SM (1988) Anal Chem 60:1639. doi:10.1021/ac00166a037
5. Bancroft EE, Sidwell JS, Blount HN (1981) Anal Chem 53:1390. doi:10.1021/ac00232a021
6. Astuti Y, Topoglidis E, Briscoe PB, Fantuzzi A, Gilardi G, Durrant JR (2004) J Am Chem Soc 126:8001. doi:10.1021/ja0496470
7. Astuti Y, Topoglidis E, Gilardi G, Durrant JR (2004) Bioelectrochemistry 63:55. doi:10.1016/j.bioelechem.2003.09.014
8. Scholz F, Meyer B (1994) Chem Soc Rev 23:341. doi:10.1039/cs9942300341
9. Hogan CF, Bond AM, Neufeld AK, Connelly NG, Llamas-Rey E (2003) J Phys Chem A 107:1274. doi:10.1021/jp027529y
10. Keane L, Hogan C, Forster RJ (2002) Langmuir 18:4826–4833. doi:10.1021/la010927s
11. Neufeld AK, Madsen I, Bond AM, Hogan CF (2003) Chem Mater 15:3573. doi:10.1021/cm0341336
12. Marken F, Cromie S, McKee V (2003) J Solid State Electrochem 7:141
13. Bond AM, Marken F, Hill E, Compton RG, Hügel H (1997) J Chem Soc, Perkin Trans 2:1735. doi:10.1039/a701003f
14. Meyer B, Ziemer B, Scholz F (1995) J Electroanal Chem 392:79. doi:10.1016/0022-0728(95)04028-M
15. Schroder U, Scholz F (1997) J Solid State Electrochem 1:62. doi:10.1007/s100080050023
16. Ramaraj R, Kabbe C, Scholz F (2000) Electrochem Commun 2:190. doi:10.1016/S1388-2481(00)00005-9
17. Forster RA, Hogan CF (2000) Anal Chem 72:5576. doi:10.1021/ac000605d
18. Bolink HJ, Cappelli L, Coronado E, Graetzel M, Nazeeruddin MK (2006) J Am Chem Soc 128:46. doi:10.1021/ja0565065
19. Klimant I, Wolfbeis OS (1995) Anal Chem 67:3160. doi:10.1021/ac00114a010
20. Rudolph M (2003) J Electroanal Chem 543:23. doi:10.1016/S0022-0728(02)01257-3
21. Kllmant I, Wolfbeis OS (1995) Anal Chem 67:3160–3166. doi:10.1021/ac00114a010
22. Cave GWV, Raston CL (2001) J Chem Soc, Perkin Trans 1:3258
23. Kronhnke F (1976) Synthesis 1. doi:10.1055/s-1976-23941
24. Constable EC, Thompson MWC (1996) N J Chem 20:65
25. Baba AI, Wang W, Kim WY, Strong L, Schmehl RH (1994) Synth Commun 24:1029. doi:10.1080/00397919408020779
26. Juris A, Balzani V (1988) Coord Chem Rev 84:85. doi:10.1016/0010-8545(88)80032-8
27. Bard AJ, Faulkner LR (eds) (2000) Electrochemical methods: fundamentals and applications. Wiley, New York
28. The blocked right boundary (BRB) condition was specified, i.e. no concentration gradient at the right-hand boundary